

Evaporation: The change from accretion via a thin disk to a coronal flow

F. Meyer¹, B.F. Liu^{1,2}, E. Meyer-Hofmeister¹

¹ Max-Planck-Institut für Astrophysik, Karl Schwarzschildstr. 1, D-85740 Garching, Germany

² Yunnan Observatory, Chinese Academy of Sciences. P.O.Box 110, Kunming 650011, China

Received:s / Accepted:

Abstract. We present a model for a corona above a geometrically thin standard disk around a black hole. This corona is fed by matter from the thin disk which evaporates from the cool layers underneath. An equilibrium establishes between the cool accretion stream and the hot flow. In the inner region evaporation becomes so efficient that at low accretion rates all matter flows via the corona and proceeds towards the black hole as an advection-dominated accretion flow (ADAF). We investigate this transition for accretion disks around stellar black holes. We derive a set of four ordinary differential equations which describe the relevant processes and solve them numerically. The evaporation efficiency has a maximum value where the advection-dominated structure of the corona (at large distances from the black hole) changes to a radiation-dominated structure (at small distances). This maximum can be related to the observed spectral transitions in black hole X-ray binaries. Our solutions of coronal structure are valid for both, accretion in galactic X-ray transients and in AGN.

Key words: accretion disks – black hole physics – X-rays: stars – stars: individual: Cygnus X-1, Nova Muscae 1991 – galaxies: nuclei

1. Introduction

Recently a wealth of X-ray observations has provided more detailed information about spectra of X-ray sources and short-time variability. This concerns soft X-ray transients as good examples of stellar accreting black holes, high-mass X-ray binaries with a black hole primary star and also Active Galactic Nuclei. The new observations put more stringent constraints on the modelling of accretion processes. In this connection the change from accretion in a standard cool disk to a hot coronal flow is an important feature.

Different solutions of accretion on to compact objects had been investigated in the past. An account can be

Send offprint requests to: Emmi Meyer-Hofmeister
e-mail: emm@mpa-garching.mpg.de

found in the review by Narayan et al. (1998). The description of an optically thick, geometrically thin disk, now often called “standard thin disk”, goes back to work of Shakura & Sunyaev (1973), Novikov & Thorne (1973), Lynden-Bell & Pringle (1974) and others. A much hotter self-consistent solution of optically thin gas was discovered by Shapiro, Lightman & Eardley (1976), but found to be thermally unstable by Piran (1978). A solution for even super-Eddington accretion rates in which the large optical depth of the inflowing gas prevents radiation to escape was suggested by Katz (1977), Begelman (1978), Abramowicz et al. (1988) and others. This is an optically thick advection-dominated accretion flow. The fourth solution concerns accretion at low sub-Eddington rate (proposed by Shapiro et al. 1976, Ichimaru 1977 and Rees et al. 1982). Detailed theoretical work on this solution by several authors has proven that this optically thin regime of solutions for low accretion rates is relevant for accretion in many cases (Narayan & Yi 1994, 1995a,b, Abramowicz, Chen & Kato et al. 1995, Chen 1995; Chen et al. 1995, 1997; Honma 1996; Narayan, Kato & Homma 1997a; Nakamura et al. 1996, 1997).

The model of an optically thin advection-dominated flow (ADAF) allows to explain the accretion in soft X-ray transients during quiescence. Assuming the old picture of a standard thin accretion disk reaching inward towards the black hole the amount of X-ray flux is clearly inconsistent with the accretion rate estimated from the outer optically thick disk (McClintock et al. 1995). An interior ADAF allows to understand the observations but requires the change from a standard thin disk to the hot flow at a certain transition radius. The black hole X-ray transients are a laboratory for accretion on to black holes. The physics of the accretion processes around supermassive black holes in AGN is similar, which makes the investigation of ADAF even more important and fruitful.

The change from a geometrically thin disk to the hot flow is an essential feature in this overall picture of accretion. The “strong ADAF principle”, formulated by Narayan & Yi (1995b), suggests that, whenever the accreting gas has a choice between a standard thin disk and an ADAF, the ADAF configuration is chosen. This rule

provides a transition radius r_{tr} for a given accretion rate (see Fig. 6b in Esin et al. 1997). In a different approach Honma (1996) considered the interface of a hot optically thin disk with a cool standard thin disk applying radial diffusive transport of heat.

Here we present a model of a corona above a thin disk in order to determine the inner edge of the thin disk, inside of which only a hot optically thin flow exists. The co-existence of a cool disk and a corona had been investigated for disks in dwarf nova systems, where features otherwise not understood as for example the X-rays observed in quiescence can then be explained (Meyer & Meyer-Hofmeister 1994, Liu et al. 1995). The situation is the same in disks around black holes (Meyer 1999), both stellar and super-massive.

The physical two-dimensional situation would demand the solution of a set of partial differential equations in radial distance r and vertical height z . In particular a sonic transition would require treatment of a free boundary condition on an extended surface. In Sect. 2 we show how we derive a simplified set of four ordinary differential equations which describe the physics of the corona above the thin disk. The interaction of corona and thin disk results in evaporation of matter from the thin disk. In Sect. 3 we discuss the general features of this evaporation process. The results of our computations are presented in Sect. 4. The main result of this model is the efficiency of evaporation and with this the location where the thin disk has completely changed to a hot coronal flow (Sect. 5). In Sect. 6 we point out the invariance of our results for different black hole masses. Sects. 7 and 8 concern the validity of the assumptions made in our computations and the importance of synchrotron and Compton processes. In Sect. 9 the comparison with observations follows, in Sect. 10 a discussion of further effects. In Sect. 11 we compare with the model of Honma (1996). Sect. 12 contains our conclusions.

2. The equations

In this section we derive the equations that describe the corona above the inner rim of the accretion disk. For this we will average over an inner ring area and thereby reduce the set of partial differential equations to a system of ordinary differential equations with respect to height. The solutions then become a function of the radial coordinate of the inner rim.

We start with the five equations of viscous hydrodynamics, conservation of mass

$$\frac{\partial \rho}{\partial t} + \nabla \cdot (\rho \mathbf{v}) = 0, \quad (1)$$

the equations of motion

$$\rho \left[\frac{\partial \mathbf{v}}{\partial t} + (\mathbf{v} \cdot \nabla) \mathbf{v} \right] = -\nabla P + \nabla \cdot \mathbf{S} - \rho \nabla \Phi, \quad (2)$$

and the first law of thermodynamics

$$\rho \left[\frac{\partial U}{\partial t} + (\mathbf{v} \cdot \nabla U) \right] = -P(\nabla \cdot \mathbf{v}) + (\mathbf{S} \cdot \nabla) \cdot \mathbf{v} + \dot{q}, \quad (3)$$

supplemented by the equation of state for an ideal gas

$$P = \frac{\Re}{\mu} T \rho, \quad (4)$$

$$U = \frac{1}{\gamma - 1} \frac{P}{\rho}, \quad (5)$$

$$\frac{\Re}{\mu} T = V_s^2. \quad (6)$$

Here ρ , P and T are density, pressure and temperature, \mathbf{v} is the velocity vector, \mathbf{S} the viscous stress tensor, Φ the gravitational potential, U the internal energy, \Re the gas constant, μ the molecular weight. We take $\mu = 0.62$ for a fully ionized gas of cosmic abundances. V_s is the isothermal speed of sound, γ the ratio of the specific heats, $= \frac{5}{3}$, for a mono-atomic gas. For \mathbf{S} we take the form appropriate for a mono-atomic gas with Cartesian components

$$\sigma_{ik} = \mu_v \left[\frac{\partial v_i}{\partial x_k} + \frac{\partial v_k}{\partial x_i} - \frac{2}{3} \delta_{ik} \frac{\partial v_l}{\partial x_l} \right] \quad (7)$$

(Sommerfeld 1949). For the (non-molecular) viscosity we use an α -parameterization (Shakura & Sunyaev 1973, Novikov & Thorne 1973)

$$\mu_v = \frac{2}{3} \alpha P / \Omega, \quad (8)$$

Ω rotational frequency. \dot{q} is the rate of heating per unit volume. We write it in two parts,

$$\dot{q} = \dot{q}_{\text{rad}} + \dot{q}_{\text{cond}}$$

where \dot{q}_{rad} is the gain or loss of heat by radiation and \dot{q}_{cond} that by heat conduction

$$\dot{q}_{\text{cond}} = -\nabla \cdot \mathbf{F}_c \quad (9)$$

For \dot{q}_{rad} we take here optically thin thermal radiation loss according to Fig. 1 of Raymond et al. (1976).

$$\dot{q}_{\text{rad}} = -n_e n \Lambda(T) \quad (10)$$

where n_e and n are electron and ion particle densities. For the heat flux \mathbf{F}_c we take

$$\mathbf{F}_c = -\kappa_0 T^{5/2} \nabla T; \quad (11)$$

(Spitzer 1962) for a fully ionized plasma and use the value

$$\kappa_0 = 10^{-6} \frac{\text{g cm}}{\text{s}^3 \text{K}^{7/2}}$$

neglecting a weak logarithmic dependence on electron density and temperature.

Taking the scalar product of Eq.(2) with \mathbf{v} , adding to Eq.(3), and using Eq.(1) we obtain the equation of conservation of energy

$$\frac{\partial}{\partial t} \left[\rho \left(U + \frac{v^2}{2} + \Phi \right) \right] + \nabla \cdot \left[\mathbf{v} \left(\rho U + \rho \frac{v^2}{2} + \rho \Phi + P \right) - (\mathbf{S} \cdot \mathbf{v}) + \mathbf{F}_c \right] = \dot{q}_{rad} \quad (12)$$

We introduce cylindrical coordinates, r, φ, z with the z -axis perpendicular to the midplane of the disk and through the central accretor, and use the vector correspondence to the Cartesian advection term

$$(\mathbf{v} \cdot \nabla) \mathbf{v} = \nabla \frac{v^2}{2} - \mathbf{v} \times (\nabla \times \mathbf{v}), \quad (13)$$

where $v^2 \equiv (\mathbf{v} \cdot \mathbf{v})$. The (Newtonian) potential is then

$$\Phi = -\frac{GM}{(r^2 + z^2)^{1/2}} \quad (14)$$

with G the gravitational constant and M the central mass.

We consider from now on stationary, azimuthally symmetric flows.

In the following subsections we derive values for the rotational velocity v_φ and the radial diffusive velocity v_r , and the three remaining ordinary differential equations for the conservation of mass, the vertical dynamic equilibrium, and the energy flow in the corona above the inner zone of the accretion disk.

For this we choose a region between inner disk radius r_1 and radius r_2 such that

$$\pi(r_2^2 - r_1^2) = \pi r^2, \quad (15)$$

where r is an area weighted mean radius between r_1 and r_2 . We apply therefore, at each radius r , the integration bounds $r_1=0.72r$ and $r_2=1.23r$. The coronal solution depends on the value of r as a measure of the distance from the accretor.

We estimate the relative order of magnitude of the various terms in our equations and drop non-dominant terms. For these estimates we use relations that result from our solutions which are therefore self-consistent.

All our solutions have

$$\frac{\Re/\mu T r}{GM} = \frac{V_s^2 r}{GM} \leq 1/8, \quad (16)$$

see Fig. 3. They are subvirial and therefore like ‘‘slim’’ accretion disks (Abramowicz et al. 1988) with cylindrical symmetry in their (main) part in contrast to the more spherical symmetry of ADAF solutions. As a result

$$\left| \frac{v_r}{v_\varphi} \right| \approx \alpha \frac{V_s^2}{v_\varphi^2} \leq \frac{\alpha}{8}, \quad (17)$$

where we have replaced the azimuthal velocity by its Kepler value which is a good approximation in the main body

of our solution, see the remark following Eq. 25 below. A wind from such a corona reaches escape speed at large height leading to

$$v_z \leq V_s \frac{z}{2r}, \quad (18)$$

see Fig. 2. Where in the following we neglect radial derivatives of velocity components we use the order of magnitude relation

$$\frac{\partial v}{\partial r} = O\left(\frac{v}{r}\right). \quad (19)$$

2.1. The r -component of the equation of motion

This equation yields the rotational velocity.

The radial component of the equation of motion becomes

$$\rho \left(v_r \frac{\partial v_r}{\partial r} + v_z \frac{\partial v_r}{\partial z} - \frac{v_\varphi^2}{r} \right) = -\frac{\partial P}{\partial r} - \rho \frac{GM r}{(r^2 + z^2)^{3/2}} + \frac{1}{r} \frac{\partial}{\partial r} (r \sigma_{rr}) + \frac{\partial}{\partial z} \sigma_{rz} \quad (20)$$

In this equation the pressure term $\partial P/\partial r$ is small compared to the gravitational term in regions $z \leq r/2$ dominant with respect to dynamics and energetics of the solutions (see Fig. 2). Taking $\partial P/\partial r = O(P/r)$ we estimate

$$\left| \frac{\partial P}{\partial r} \right| / \frac{\rho GM r}{(r^2 + z^2)^{3/2}} \approx \frac{V_s^2 r}{GM} \left(1 + \frac{z^2}{r^2} \right)^{3/2} \leq \frac{1}{8} \left(1 + \frac{z^2}{r^2} \right)^{3/2} \leq 0.18 \quad (21)$$

This shows a relative unimportance of radial pressure support in these coronae (in contrast to virialized ADAF solutions, Narayan & Yi (1995b)). At a large height $z = r$ this ratio has increased to 0.35. But we note that with the topology of Fig. 1 that at that height the radial pressure gradient must have significantly decreased because of the axial geometry. Therefore to first approximation we can neglect the pressure term.

The viscous terms

$$\sigma_{rr} = \mu_v \left(2 \frac{\partial v_r}{\partial r} - \frac{2}{3} \nabla \cdot \mathbf{v} \right), \quad \sigma_{rz} = \mu_v \left(\frac{\partial v_r}{\partial z} + \frac{\partial v_z}{\partial r} \right) \quad (22)$$

contribute derivatives of r - and z -components of the velocity. Their contributions, evaluated with Eqs. (16) to (19), are small compared to

$$\frac{\partial P}{\partial r} \approx O(P/r) \quad (23)$$

by at least a factor V_s/v_φ . They as well as the first two terms on the left hand side of Eq. (20) are negligible.

This leaves the balance between centrifugal and radial gravitational force

$$v_\varphi^2 = \frac{GM}{r} \left(1 + \frac{z^2}{r^2}\right)^{-3/2} \quad (24)$$

$$\Omega = \sqrt{\frac{GM}{r^3}} \left(1 + \frac{z^2}{r^2}\right)^{-3/4} \quad (25)$$

In the main body of the coronal solution the Kepler values (i.e. at $z=0$) are a good approximation to v_φ and Ω . In our calculation we take the Kepler values throughout as a computational convenience. It overestimates the frictional work and underestimates the release of rotational energy at large height. These two effects partially compensate each other. At $z \leq r/2$ the sum of these effects deviates from the accurate value by less than 7%. At $z = r$ it is 20%. But at this height the total further contribution of both energy terms already is negligibly small (due to the exponential decrease of pressure and density with height, see Fig. 2) and isothermality of the solution completely dominates. This simplification has thus only a small effect on the accuracy of the solution.

2.2. The φ -component of the equation of motion

The conservation of the z -component of angular momentum yields the r -component of the velocity.

Multiplication of the equation of motion by $r \mathbf{u}_\varphi$ ($\mathbf{u}_r, \mathbf{u}_\varphi, \mathbf{u}_z$ unit vectors in r, φ and z direction) yields

$$\begin{aligned} \rho \mathbf{v} \cdot \nabla (r v_\varphi) &= r \mathbf{u}_\varphi \cdot (\nabla \cdot \mathbf{S}) \\ &= \nabla \cdot (\mathbf{S} \cdot r \mathbf{u}_\varphi) - (\mathbf{S} \cdot \nabla) r \mathbf{u}_\varphi \end{aligned} \quad (26)$$

Using (1) (for $\frac{\partial}{\partial t} = 0$)

$$\nabla \cdot \rho \mathbf{v} = 0,$$

and

$$\nabla r \mathbf{u}_\varphi = \mathbf{u}_r \mathbf{u}_\varphi - \mathbf{u}_\varphi \mathbf{u}_r,$$

(the right side understood as the dyadic product) and

$$\sigma_{r\varphi} = \sigma_{\varphi r},$$

this results in the equation of conservation of z -angular momentum

$$\nabla \cdot (\rho \mathbf{v} r v_\varphi - r \mathbf{u}_\varphi \cdot \mathbf{S}) = 0. \quad (27)$$

We integrate over a cylinder with radius r_1 and obtain

$$2\pi r_1^2 \int_0^\infty \rho v_r v_\varphi dz = 2\pi r_1^2 \int_0^\infty \sigma_{r\varphi} dz. \quad (28)$$

Here it is assumed that no significant angular momentum is accreted at the center of the compact object or lost through the boundary $z = \infty$. For accretion and jet

angular momentum loss from the most interior parts of the accretion region, such losses would be small by order of $\sqrt{R/r_1}$ where R is the radius of the inner accretion region, e.g. $R \approx 3r_S$ for the Schwarzschild radius r_S of a central black hole ($r_S = 2GM/c^2$).

We replace the global balance of angular momentum flow of Eq. (28) by its local equivalent and obtain the radial diffusive velocity

$$v_r = \frac{\sigma_{r\varphi}}{\rho v_\varphi} = -\alpha \frac{V_s^2}{v_\varphi} \quad (29)$$

with $\sigma_{r\varphi} = \mu_v (\partial v_\varphi / \partial r - v_\varphi / r) = -\alpha P$. This is the standard bulk radial velocity formula for accretion disks. It neglects the modification by z -dependent secondary flows superimposed on the main drift of material (see Kley & Lin 1992). Such secondary flows may slightly modify the local vertical structure but will hardly affect the general structure of the solutions.

2.3. The z -component of the equation of motion

The vertical component of the equation of motion Eq. (2) yields the vertical dynamic equilibrium.

The vertical component becomes

$$\begin{aligned} \rho (v_r \frac{\partial v_z}{\partial r} + v_z \frac{\partial v_z}{\partial z}) &= -\frac{\partial P}{\partial z} - \rho \frac{GMz}{(r^2 + z^2)^{3/2}} \\ &+ \frac{1}{r} \frac{\partial}{\partial r} (r \sigma_{rz}) + \frac{\partial}{\partial z} \sigma_{zz}. \end{aligned} \quad (30)$$

Using approximate isothermal pressure layering (see Fig. 2)

$$P = P_0 e^{-(z/h)^2} \quad (31)$$

with $h \approx \frac{1}{2}r$ (see Fig. 3) and the estimates of Eqs. (16) to (19) we estimate

$$\left| \rho v_r \frac{\partial v_z}{\partial r} \right| \left| \frac{\partial P}{\partial z} \right| \leq 0.02\alpha \quad (32)$$

to be negligible. Further, with

$$\sigma_{rz} = \mu_v \left(\frac{\partial v_r}{\partial z} + \frac{\partial v_z}{\partial r} \right), \sigma_{zz} = \mu_v \left(2 \frac{\partial v_z}{\partial z} - \frac{2}{3} (\nabla \cdot \mathbf{v}) \right) \quad (33)$$

the largest contribution of all viscous terms in Eq. (30) appears in $\partial \sigma_{zz} / \partial z$ from the z -derivative of μ_v (that is of P , see Eq. (8) times the derivative $\partial v_z / \partial z$). This term is of order $\leq 0.16\alpha \approx 0.05$ and negligible. In the remaining dominant terms only z -derivatives appear. Averaging over the inner zone we obtain

$$\rho v_z \frac{dv_z}{dz} = -\frac{dP}{dz} - \rho \frac{GMz}{(r^2 + z^2)^{3/2}}. \quad (34)$$

2.4. Mass conservation

The equation of mass conservation we integrate over the radial zone between r_1 and r_2 , of area πr^2 and obtain

$$\int_{r_1}^{r_2} 2\pi r \frac{\partial}{\partial z} (\rho v_z) dr = (2\pi r \rho v_r)_1 - (2\pi r \rho v_r)_2. \quad (35)$$

When, as we assume, $r \rho v_r$ drops off with radius strongly (e.g. $\rho \sim r^{-3}$ in the scaled solutions, Liu et al. 1995) the difference on the right hand side is dominated by the first term, and its value will be slightly smaller than this term. We approximately take this into account by replacing the term at r_1 by its value at the somewhat larger mean radius r . We replace the left hand side by the area times a mean value. This leads to the approximation

$$\frac{d}{dz} (\rho v_z) = \frac{2}{r} \rho v_r \quad (36)$$

where v_r is the radial flow velocity (Eq. 29). At large height, however, we have to take into account the flaring of the channel as the ascending gas changes from a cylindrical rise to spherical expansion (see Fig. 1). How can we account for the additional attenuation of the vertical flux density by this change of geometry?

We proceed in the following way. Approximately the cross section of the vertical flow channel can be taken as proportional to $1 + z^2/r^2$. Without sidewise diffusive loss, mass conservation would then yield

$$\frac{d}{dz} \left[\left(1 + \frac{z^2}{r^2} \right) \rho v_z \right] = 0 \quad (37)$$

if we take the center of the expanding flux tube in the vertical direction. Per unit cross section the resulting conservation equation is then

$$\frac{1}{1 + \frac{z^2}{r^2}} \frac{d}{dz} \left[\left(1 + \frac{z^2}{r^2} \right) \rho v_z \right] = \frac{d}{dz} (\rho v_z) + \frac{2z}{r^2 + z^2} \rho v_z = 0 \quad (38)$$

The gas in a cylindrical column thus experiences an additional geometry-related radial divergence

$$-\frac{2z}{(r^2 + z^2)} \rho v_z$$

Adding the two radial flow components we obtain the final form

$$\frac{d}{dz} (\rho v_z) = \frac{2}{r} \rho v_r - \frac{2z}{r^2 + z^2} \rho v_z \quad (39)$$

We note that the diffusive part in this equation becomes unimportant at large height where the diffusive description for the flaring flux tube becomes problematic.

2.5. Energy conservation

We first derive the frictional flux terms. With Eqs. (22) and (13) we obtain

$$(\mathbf{v} \cdot \mathbf{S}) = \mu_v \left[\nabla v^2 - \mathbf{v} \times (\nabla \times \mathbf{v}) - \frac{2}{3} \mathbf{v} (\nabla \cdot \mathbf{v}) \right] \quad (40)$$

and its r -component

$$\mathbf{u}_r \cdot (\mathbf{v} \cdot \mathbf{S}) = \mu_v \left[\frac{\partial v^2}{\partial r} - v_\varphi \frac{\partial v_\varphi}{\partial r} - \frac{v_\varphi^2}{r} + v_z \left(\frac{\partial v_r}{\partial z} - \frac{\partial v_z}{\partial r} \right) - \frac{2}{3} v_r \nabla \cdot \mathbf{v} \right] \quad (41)$$

Here all terms are negligible except those containing v_φ , by use of Eqs. (16) to (19). Making use of Eqs. (8) and (19) we obtain

$$\mathbf{u}_r \cdot (\mathbf{v} \cdot \mathbf{S}) = -\alpha P v_\varphi. \quad (42)$$

Likewise, only keeping non-negligible v_φ - terms, the z -component is

$$\mathbf{u}_z \cdot (\mathbf{v} \cdot \mathbf{S}) = \mu_v \left[\frac{\partial v^2}{\partial z} - v_r \left(\frac{\partial v_r}{\partial z} - \frac{\partial v_z}{\partial r} \right) - v_\varphi \frac{\partial v_\varphi}{\partial z} - \frac{2}{3} v_z (\nabla \cdot \mathbf{v}) \right] = \frac{2}{3} \alpha P r \frac{\partial v_\varphi}{\partial z}. \quad (43)$$

The radial component of the divergence can be written, using (19) as

$$\frac{1}{r} \frac{\partial}{\partial r} [r \mathbf{u}_r \cdot (\mathbf{v} \cdot \mathbf{S})] = -\alpha P \Omega \left(\frac{1}{2} + \frac{\partial \ln P}{\partial \ln r} \right) = \frac{3}{2} \alpha P \Omega. \quad (44)$$

For $\partial \ln P / \partial \ln r$ we have here taken its estimated value -2 at the characteristic height $z = h = r/2$ (see Fig. 2), which we obtain from Eq. (31) with the scaling $P_0 \sim r^{-4}$ that holds when we compare solutions with different distances r (see Liu et al. 1995). The resulting term represents the dominant heating mechanism of the corona by release of gravitational energy.

We now integrate over the area between r_1 and r_2 as in the derivation of conservation of mass

$$\begin{aligned} & \int_{r_1}^{r_2} 2\pi r dr \left\{ \frac{\partial}{\partial z} \left[v_z \left(\rho \frac{v^2}{2} + \frac{\gamma}{\gamma-1} P + \rho \Phi \right) \right. \right. \\ & \quad \left. \left. + (F_c)_z + \frac{2}{3} \alpha P r \frac{\partial v_\varphi}{\partial z} \right] - \frac{3}{2} \alpha P \Omega - \dot{q}_{rad} \right\} \\ & = \left\{ 2\pi r \left[v_r \left(\rho \frac{v^2}{2} + \frac{\gamma}{\gamma-1} P + \rho \Phi \right) + (F_c)_r \right] \right\}_{r_1} \\ & \quad - \left\{ \dots \right\}_{r_2} \end{aligned} \quad (45)$$

On the right hand side of this equation we again replace the difference of the terms taken at r_1 and r_2 by the value taken at the intermediate value r , because the value at r_2 will only be a fraction of the value at r_1 due to the radial drop off of all the quantities. If we take v_r as the diffusive velocity (Eq. (29)) we must still include the divergence of the vertical flow due to the flaring geometry. We use the same procedure as in the preceding Sect. 2.4 to derive the corresponding term and add it on the right hand side. Again, on the left hand side of the equation we write the integral as area times a mean value and obtain the energy equation in its final form

$$\begin{aligned} \frac{d}{dz} \left[v_z \left(\rho \frac{v^2}{2} + \frac{\gamma}{\gamma-1} P + \rho \Phi \right) + \frac{2}{3} \alpha P r \frac{dv_\varphi}{dz} + (F_c)_z \right] = \\ \frac{3}{2} \alpha P \Omega + \dot{q}_{rad} \\ + \frac{2}{r} \left[v_r \left(\rho \frac{v^2}{2} + \frac{\gamma}{\gamma-1} P + \rho \Phi \right) + (F_c)_r \right] \\ - \frac{2z}{r^2 + z^2} \left[v_z \left(\rho \frac{v^2}{2} + \frac{\gamma}{\gamma-1} P + \rho \Phi \right) \right. \\ \left. + \frac{2}{3} \alpha P r \frac{dv_\varphi}{dz} + (F_c)_z \right]. \end{aligned} \quad (46)$$

Had we chosen to integrate the radial divergence $\frac{1}{r} \frac{\partial}{\partial r} [r \mathbf{u}_r \cdot (\mathbf{v} \cdot \mathbf{S})]$ underneath the integral of Eq. (45) instead of evaluating this term as in Eq. (44) the last equation would have the factor 2 instead of $\frac{3}{2}$. This difference arises from the different assumptions about radial variation of the quantities, implicit in the two approaches. It shows a natural limit of numerical accuracy of any such approach.

The lateral inflow of heat by $(F_c)_r$ adds to the frictional release of energy in the coronal column. We show that the relative size of the contribution is small and we will take $(F_c)_r=0$ in our computations. We assume that the temperature at low z/r varies like the virial temperature, $T \sim 1/r$, and that at $z \geq r$ the radial temperature gradient becomes small as the topology changes and the corona fills the full cylindrical region, with $\frac{\partial T}{\partial r} = 0$ on the axis of symmetry. With these assumptions we take

$$\frac{\partial T}{\partial r} = \frac{T}{r} \left(1 - \frac{z^2}{r^2} \right). \quad (47)$$

The ratio of total radial conductive heat input $(\dot{Q}_c)_r$ to the total frictional energy input \dot{Q}_f is then evaluated as

$$\begin{aligned} \frac{(\dot{Q}_c)_r}{\dot{Q}_f} \\ = \int_0^{z_0} \frac{1}{r} \frac{\partial}{\partial r} [r(F_c)_r] dz / \int_0^{z_0} \frac{3}{2} \alpha P \Omega dz = 0.22, \end{aligned} \quad (48)$$

It is independent of the value of r as long as we are in the ‘‘advection-dominated’’ range $r \geq r(\dot{M}_{\text{crit}})$ (see Fig.3).

This follows when one uses the scaling of P , T and Ω derived by Liu et al. (1995) (see also values P_0 in Table 1). In the ‘‘conduction-dominated’’ corona $r \leq r(\dot{M}_{\text{crit}})$ the temperature becomes constant and the ratio becomes zero. The contribution of $(F_c)_r$ can therefore be neglected. The remaining z -component of Eq. (11) we write as

$$F_c \equiv (F_c)_z = -\kappa_0 T^{5/2} \frac{dT}{dz} \quad (49)$$

2.6. The system of ordinary differential equations with boundary conditions

From the five partial differential equations (1) to (3) we have now derived three ordinary differential equations (34), (39) and (46) (where we take $(F_c)_r = 0$) which describe vertical dynamical equilibrium and conservation of mass and energy, plus the two expressions for v_φ and v_r (Eqs. (24) and (29)). Our fourth ordinary differential equation is the dependence of the heat flux on the temperature gradient, Eq. (49). As the 4 dependent variables we have temperature T , pressure P , mass flow $\dot{m} = \rho v_z$ and heat flux F_c . The 4 boundary conditions are:

(1) No pressure at infinity (i.e. no artificial confinement). This requires sound transition at some height $z = z_1$ (free boundary problem)

$$v_z = V_s \quad \text{at} \quad z = z_1. \quad (50)$$

(2) No influx of heat from infinity. We neglect a small outward conductive heat flux induced by the temperature gradient in the expanding wind and require

$$F_c = 0 \quad \text{at} \quad z = z_1. \quad (51)$$

(3) Chromosphere temperature at the bottom $z = z_0$

$$T = T_{\text{eff}} \quad \text{at} \quad z = z_0. \quad (52)$$

(4) No heat inflow at the bottom

$$F_c = 0 \quad \text{at} \quad z = z_0. \quad (53)$$

This approximates the condition that the chromospheric temperature is kept up by other processes and cannot conduct any sizeable thermal heat flow.

The consequence of conditions (3) and (4) is that the conductive flux that comes down at a certain level above the boundary must be radiated away. Since the advective cooling by the rising mass flow is small (in our solutions at $T^{6.5} \text{K}$ only $\frac{1}{10}$) this reduces to the balance between thermal conductive flux and radiation and establishes the temperature profile as the one studied by Shmeleva & Syrovatskii (1973) for the solar corona. In these lowest layers the pressure is nearly constant and the temperature rises steeply. Liu et al. (1995) recalculated the temperature profile using the more recent cooling function of Raymond et al. (1976) and we used the improved version. This allows to replace the conditions (3) and (4) by

$$T = 10^{6.5} \text{K} \quad \text{and} \quad F_c = -2.73 \cdot 10^6 \text{P} \quad \text{at} \quad z = z_0 \quad (54)$$

The relation between P and F_c is practically independent of the value of the chromospheric temperature as long as it is small compared to $T_0 = 10^6.5\text{K}$.

These equations and boundary conditions describe a model of the corona-disk interaction for the innermost region of the thin accretion disk where evaporation is most efficient.

3. General features of evaporation

The equations derived in the last section describe the physics of a hot corona in equilibrium with a thin cool disk underneath. Aspects of this model had already been investigated for accretion on to a white dwarf (Meyer & Meyer-Hofmeister 1994, Liu et al. 1995, for application to WZ Sge stars and X-ray transients see also Mineshige et al. 1998). The picture that arises from the processes involved is the following. Heat released by friction in the corona flows down into cooler and denser transition layers. There it is radiated away if the density is sufficiently high. If the density is too low, cool matter is heated up and evaporated into the corona until an equilibrium density is established. Mass drained from the corona by an inward drift is steadily replaced by mass evaporating from the thin disk as the system reaches a stationary state. This evaporation rate increases steeply with decreasing distance from the central compact star. When the evaporation rate exceeds the mass flow rate in the cool disk, a hole forms up to the distance where both rates are equal. Inside this transition radius r_{tr} only a hot coronal flow exists.

The mass flow in the corona is similar to that in the thin disk. The matter has still its angular momentum, and differential (Kepler-like) rotation causes friction. The main part of the coronal gas flows towards the center directly. For conservation of angular momentum a small part flows outward in the coronal layer and condensates in the outer cool disk. Since the temperature is very high the corona is geometrically much thicker than the disk underneath. Therefore processes as sidewise energy transport and downward heat conduction are important for the equilibrium between corona and thin disk, together with radiation and wind loss.

We model the equilibrium between corona and thin disk in a simplified way using a one-zone model as described in Sect. 2. This is possible since the evaporation process is concentrated near the inner edge of the thin disk and we can choose a representative radial region from r_1 to r_2 such that the main interaction between cool disk and corona occurs there and evaporation further outward is not important. In Fig. 1 we show the flow pattern as derived from analysis and simplified modelling for the case that a hole in the thin disk exists. There are three regimes. (1) Near the inner edge of the thin disk the gas flows towards the black hole. (2) At larger r wind loss is important taking away about 20% of the total matter inflow. (3) At even larger distances some matter flows outward

in the corona as a consequence of conservation of angular momentum. (One might compare this with the flow in a “free” thin disk without the tidal forces acting in a binary. In such a disk matter flows inward in the inner region and outward in the outer region, with conservation of the total mass and angular momentum (Pringle 1981)).

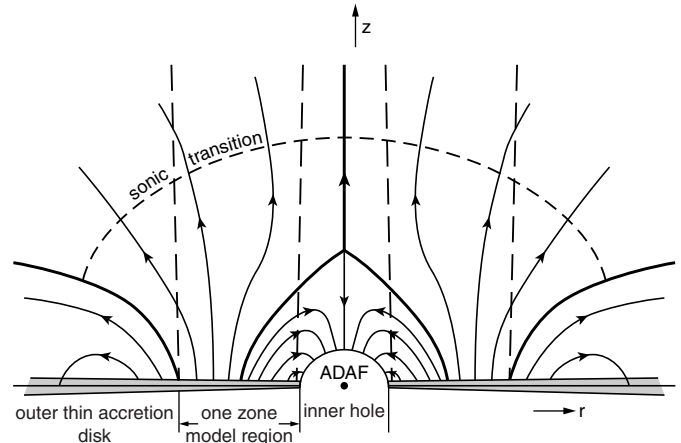


Fig. 1. Coronal mass flow pattern (schematic). Convective circulations will be superimposed.

4. Results from computations

4.1. Computer code technique

We solve the differential equations (34), (39), (46), and (49) using the Runge-Kutta method integrating from the lower boundary at an assumed height $z_0 \ll r$ above the midplane to the upper boundary at z_1 . The value z_1 is determined by our computations as the height where sound transition occurs (free boundary problem). The boundary conditions are given in Eqs. (50), (51) and (54). We require that the energy flux at the upper boundary is zero but are content in our computations if it is very small, $|F_c| \leq 0.005 \cdot |(F_c)_{\text{max}}|$.

We have to vary P_0 and \dot{m}_0 , trial values for P and \dot{m} ($\dot{m} = \rho v_z$) at $z = z_0$, to find the coronal structure which fulfills the upper boundary conditions. The conditions, sound transition and zero heat flux, are met only for a unique pair of values for pressure and mass flow at the bottom. For other values sound transition is not reached and/or the heat flux is not negligible (this is the same situation as in coronae of cataclysmic variable disks, compare Fig. 2 of Meyer & Meyer-Hofmeister 1994). Numerically, the smaller the distance r from the compact object the more accurately the pressure value has to be determined to obtain a consistent solution.

For our computations we put the lower boundary at about $z_0 = 2 \cdot 10^6 \text{cm}$ above the midplane, but for $r \leq 3 \cdot 10^8 \text{cm}$ at correspondingly smaller values z_0 . In most cases the true height of the thin disk is less than the chosen value z_0 .

We carried out test computations to check the influence of assuming different values z_0 on the coronal structure. As expected the changes were found to be very small.

P_0 and $(F_c)_0$ are nearly independent of the value of the chromospheric temperature as long as it is small compared to $T_0 = 10^{6.5}\text{K}$.

Since our results also concern accretion in AGN we have confirmed the validity of our assumption for the location of the lower boundary for this case also.

4.2. Coronal structure

We took $6M_\odot$ as our standard parameter value to model the evaporation in accretion disks around stellar black holes. We compute the structure of the corona for distances of the outer cool disk from the black hole ranging from large values to small values of a few hundred Schwarzschild radii. For different distances r the structure in z direction is similar if considered as a function of z/r . As will be discussed in Sect. 6 the coronal structure scales with Schwarzschild radius and Eddington accretion rate.

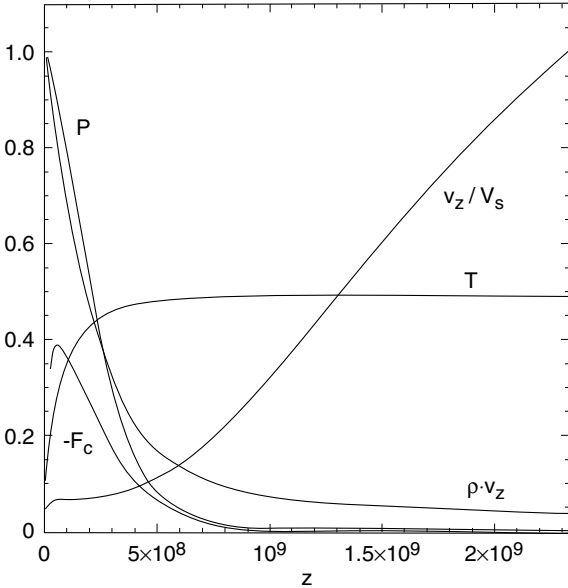


Fig. 2. Coronal structure at distance $r = 10^{8.8}\text{cm}$ from the $6M_\odot$ black hole. Temperature T is given in units of 0.2-virial temperature, pressure P and vertical mass flow $\rho \cdot v_z$ (v_z vertical velocity) are scaled to their values at the lower boundary. $-F_c$ is the downward conductive heat flux, measured in units of the frictional energy generation rate in a column of unit cross section. V_s is the sound velocity.

In Fig. 2 we show the structure at $r = 10^{8.8}\text{cm}$ close to where the evaporation efficiency is highest for a $6M_\odot$ black hole. Pressure and density decrease significantly within a narrow range above the cool disk. The downward conductive heat flux $-F_c$ therefore also has its maximum at a low

height z , then rapidly decreases with height and is negligibly small where sound transition $v_z/V_s = 1$ is reached, our boundary conditions. This happens at $2.3 \cdot 10^9\text{cm}$. The temperature is practically constant in the higher layers of the corona, a consequence of the high thermal conductivity. The computed coronal structure at distance r corresponds to the situation that the cool disk underneath extends from this distance r (inner edge) outwards. The derivation in Sect. 2 is based on the dominant role of the innermost corona and our model cannot be used to describe the coronal structure above the cool thin disk farther out which will be affected by the dominant process farther in.

These results can be compared to those of our earlier investigation of evaporation in cataclysmic variable disks. The coronal structure was considered there at distances $10^{8.7}$ to $10^{9.7}\text{cm}$ from the $1M_\odot$ white dwarf adequate for a disk around a white dwarf. Due to the scaling with the mass of the compact star the structure above the thin disk around a $1M_\odot$ white dwarf at distances $\log r$ 9.0 and 9.7 (shown in Liu et al. 1995, Fig. 1a and 1b) corresponds to the structure at distances $\log r/r_s = 3.53$ and 4.23 from a $6M_\odot$ black hole.

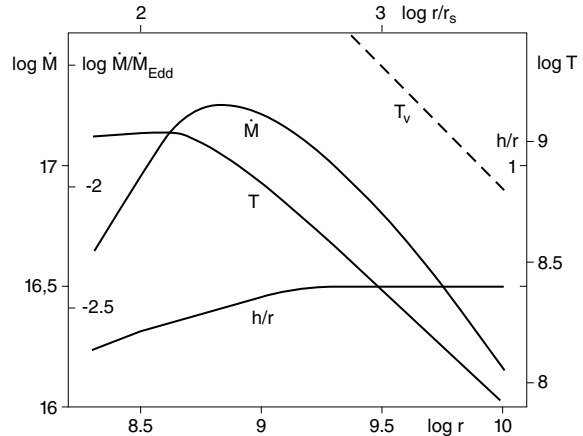


Fig. 3. Values of quantities at the inner edge $r=r_{\text{tr}}$ of the thin disk for various distances r (in cm). Rate of inward mass flow \dot{M} (in g/s) in the corona (= evaporation minus wind loss), maximum temperature in the corona and h/r (h pressure scaleheight), solid lines. Dashed line: virial temperature. Values of \dot{M} and r are for a central mass of $6M_\odot$, scaling with \dot{M}_{Edd} and r_s is indicated.

With distance from the black hole the coronal structure changes. The main result concerns the evaporation rate, the shape of the function \dot{M} . For small values of r the evaporation rate \dot{M} increases with r , then reaches a maximum value and decreases further outward. In Fig. 3 we show the evaporation rate, the temperature reached at sound transition and the ratio of the pressure scaleheight h to r (maximal temperature and pressure scaleheight from the computed vertical structure of the corona). In Table

Table 1. Evaporation of the disk around a black hole of $6M_{\odot}$

$\log r$	$\log \dot{m}_0$	$\log P_0$	$T(\text{K})$	$\dot{M} = 2\pi r^2 \dot{m}_0 (M_{\odot}/y)$	λ	$\log r/r_S$	$\dot{M}/\dot{M}_{\text{Edd}}$
10	-4.644	4.140	8.00×10^7	2.263×10^{-10}	0.211	3.75	1.712×10^{-3}
9.7	-3.646	5.302	1.55×10^8	5.657×10^{-10}	0.185	3.45	4.280×10^{-3}
9.3	-2.399	6.791	3.70×10^8	1.582×10^{-9}	0.146	3.05	1.197×10^{-2}
9.0	-1.586	7.825	6.67×10^8	2.583×10^{-9}	0.091	2.75	1.954×10^{-2}
8.9	-1.351	8.144	7.95×10^8	2.800×10^{-9}	0.066	2.65	2.118×10^{-2}
8.8	-1.143	8.445	9.28×10^8	2.852×10^{-9}	0.039	2.55	2.158×10^{-2}
8.7	-0.975	8.717	1.04×10^9	2.650×10^{-9}	0.016	2.45	2.005×10^{-2}
8.5	-0.824	9.112	1.09×10^9	1.493×10^{-9}	$\leq 10^{-3}$	2.25	1.130×10^{-2}
8.3	-0.746	9.421	1.05×10^9	7.115×10^{-10}	$\leq 10^{-3}$	2.05	5.383×10^{-3}

Note: \dot{m}_0 and P_0 vertical mass flow rate and pressure at the lower boundary z_0 , T temperature reached at the upper boundary (sound transition), \dot{M} rate of inward mass flow in the corona (=evaporation rate); λ fraction of mass carried away by the wind; quantities r/r_S and $\dot{M}/\dot{M}_{\text{Edd}}$ scaled to Schwarzschild radius and Eddington accretion rate. r, \dot{m}_0, P_0 in cgs units.

1 we summarize values of characteristic quantities. Note the large variation in the values \dot{m}_0 and P_0 , the values of P and \dot{m} at the lower boundary. The evaporation rate is given in (M_{\odot}/y) and scaled to the Eddington accretion rate ($\dot{M}_{\text{Edd}} = L_{\text{Edd}}/0.1c^2$), the radius in units of Schwarzschild radius r/r_S is added. For different black hole masses, the evaporation rate can be scaled accordingly (Sect. 6).

To include the evaporation process in the evolution of the accretion disk, e.g. for black hole X-ray transients, the \dot{M} - r relation for values r larger than the values in Fig. 3 might be needed. For such distances much larger than the hump location (Fig. 3, $\log r/r_S \geq 3$) the function \dot{M} can be approximated as found in the earlier investigation by Liu et al. (1995) for accretion in cataclysmic variables.

In Table 1 we also give the fraction of mass carried away by the wind. Note that this fraction is of the order 20% at large distances r and decreases to very small values inside the maximum of the function \dot{M} (Fig. 3). The location of sound transition is about at the height $3r$ for a distance $r = 10^{8.8}\text{cm}$, the hump location, and at increasingly larger heights further inward. But their uppermost layers are unimportant for the energy balance in the corona because of their very low density.

Disks around black holes can reach inward even to the last stable orbit, and a new feature appears, a maximum efficiency of evaporation. In dwarf nova systems the inner disk edge disk lies much further out measured in Schwarzschild radii. The maximum of the evaporation efficiency has important consequences for the inward extension of the thin disk (see Sect. 5). This maximum is caused by the change in the physical process that removes the heat released by friction. For larger radii the frictional coronal heating is balanced by inward advection and wind loss. This fixes the coronal temperature T at about 1/8 of the virial temperature T_v ($\mathcal{R}T_v/\mu = GM/r$). Downward heat conduction and subsequent radiation in the denser lower region play a minor role for the energy loss though

they always establish the equilibrium density in the corona above the disk. The ratio of the pressure scaleheight h to r is almost constant for larger r and becomes small closer to the compact object.

4.3. The energy balance in the corona

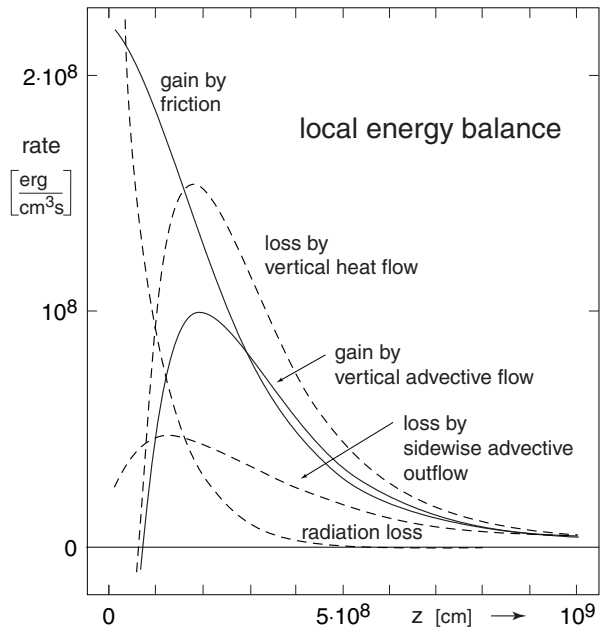


Fig. 4. Contributions to the local energy balance in the corona above the thin disk around a $6M_{\odot}$ black hole at $\log r=8.8$. Solid lines: gain by friction and vertical advective flow, dashed lines: loss by radiation, vertical heat flow and sideways advective outflow (flow out of the unit volume)

To illustrate the local energy balance we show in Fig. 4 all contributions separately as functions of height z . There are two terms of energy gain, by friction and by vertical advective flow. Friction decreases with height with the pressure (compare the coronal structure in Fig. 2). The gain by vertical advection results from the fact that more mass enters from the layer below than leaves into the layer above. This is due to the net sidewise outflow out of the unit volume. This overcompensates the increase of enthalpy with height. Concerning the losses, the radiation loss is the essential part in lower layers. It is proportional to the square of density and decreases steeply towards higher z . The loss by vertical heat flow describes the effect that the heat, released by friction and advection in higher layers is conducted down to layers where it is radiated away.

When the temperature has dropped to $10^{6.5}\text{K}$ at very low height the downward heat flow is then 10 times larger than the upward advective flow. The balance is then between conduction and radiation. This leads to the temperature profile calculated by Shmeleva & Syrovatskii (1973) and Liu et al. (1995) and fixes the relation between F_c and P at this temperature used as boundary condition for our calculations.

For $\log r=8.8$ (Fig. 4) the height-integrated losses by advective outflow and by radiation are about equal. This is a particular case. With distance r the relative size of these two losses varies in a characteristic way. To show this we have integrated the two losses over the height of the (flaring) column and normalized by the total release of energy by friction. Fig. 5 shows the result. The advective loss term includes the energy carried advectively away with the wind. This latter contribution is also shown separately.

The maximal coronal mass flow rate is reached at that radius where the character of the solution changes from an advection-dominated flow at large radii to a radiation-dominated flow at small radii (see Fig. 3). (This is an intrinsic feature of the solutions as a dimensional analysis of the global energy balance equation can show).

This behaviour contrasts with that of optically thin accretion flows of constant mass flow rate \dot{M} . These are advection-dominated (ADAF) at small radii but become radiation-dominated (Shapiro, Lightman and Eardley 1976) at large radii (Narayan & Yi 1995b). The coronal evaporation, on the other hand, allows for mass exchange between disk and corona and results in a \dot{M} varying with r which results in an inversion of that behaviour.

This mass exchange also provides thermal stability to the coronal evaporation solution. The system responds to a slight increase in temperature by an increased thermal flux that leads to an increase of density due to increased evaporation and thereby to a decrease of temperature by increased radiative cooling.

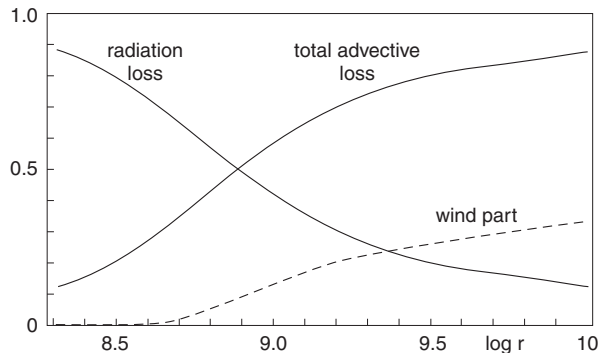


Fig. 5. Distribution of the total energy released by friction. Solid lines: fraction going into radiation and fraction removed by advection (sidewise and via the wind); dashed line: wind part only. ($6M_{\odot}$ black hole)

5. The inner edge of the thin disk and spectral transitions

If the mass flow rate in the disk is low, the evaporation rate in the inner disk region may exceed the mass flow rate. The inner edge of the cool disk then is located where both rates are equal, that is where all matter brought in by the thin disk is evaporated. Inside this location only a coronal flow exists. This coronal flow provides the supply for the ADAF towards the compact object. The higher the mass flow rate in the cool disk the further inward is the transition to a coronal flow/ADAF. This is the situation in transient black hole X-ray binaries during quiescence. If the mass flow rate exceeds the maximal evaporation rate, $\dot{M} \geq \dot{M}_{\text{crit}}$ (the peak coronal mass flow rate), the inner cool disk cannot be completely evaporated anymore, instead it reaches inward to the last stable orbit. In high-mass X-ray binaries fluctuations of the mass flow rate have the same effect. In Fig. 6 we show how the inward extent of the standard thin disk depends on the mass flow rate in the thin disk. As indicated there the corresponding spectra are hard, if the hot coronal flow/ADAF dominates, or, soft, if the standard thin disk radiation dominates near the center. This picture from our modelling is the same as the description of the accretion flow for different spectral states presented in the investigation of advection-dominated accretion by Esin et al. (1997, Fig. 1, except the very high state).

As illustrated in Fig. 5 the transition between dominant advective losses further out and dominant radiative losses further in causes the change in the slope of the evaporation rate at $\dot{M} = \dot{M}_{\text{crit}}$. Except for the difference between the sub-virial temperature of the corona and the closer-to-virial temperature of an ADAF of the same mass flow rate, a similar critical radius is then predicted by the “strong ADAF proposal” (Narayan & Yi 1995b). In general, however, the strong ADAF proposal results in an ADAF region larger than that which the evaporation

model yields. A detailed discussion of these spectral transitions was given separately (Meyer et al. 2000).

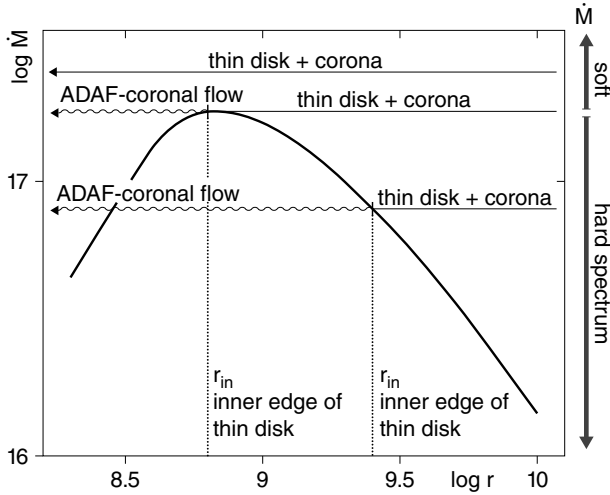


Fig. 6. Evaporation rate $\dot{M}(r)$ as in Fig. 3. Inward extension of the standard thin disk for 3 different mass flow rates \dot{M} in the thin disk (schematic). Note that the standard thin disk reaches inward towards the black hole if $\dot{M} \geq \dot{M}_{\text{crit}}$. Shown is also the type of spectrum, soft or hard, related to \dot{M}

The main results from our model are the following. The transition from a thin disk to an ADAF should occur at about the same luminosity for different systems if their black hole masses are not too different. The inner edge location should then either be at a distance of some Schwarzschild radii (the distance for which $\dot{M} = \dot{M}_{\text{crit}}$) or the thin disk should reach inward to the last stable orbit. Several high-mass binaries and black hole transients show such a systematic behaviour (Tanaka & Shibazaki 1996, Tanaka 1999). But in some cases the transition seems to be farther inward. In Sect. 9 we compare our results with observations.

6. Solutions for different central masses - stellar and supermassive black holes

Our equations and boundary conditions are invariant against scale transformations that leave temperature and velocities constant. An invariant Kepler velocity implies that M/r is invariant as is $F_c r, P r, \rho r, \dot{m} r$ and \dot{M}/r . One thus obtains solutions for another central mass M_2 from those for M_1 by multiplying r, z and \dot{M} values by M_2/M_1 , and by dividing F_c, P, ρ and \dot{m} values by the same factor while keeping velocities and temperatures the same. Since

$$\dot{M}_{\text{Edd}} = \frac{40\pi GM}{\kappa c}, \quad r_S = \frac{2GM}{c^2} \quad (55)$$

are both proportional to mass, the relation between \dot{M} and r is invariant if plotted in units of Eddington accretion rate

and Schwarzschild radius. In these units Fig. 3 is universal and applies to both stellar size and supermassive black holes.

The properties of the thin disk underneath do not scale similarly. This has no effect on the coronal structure, but shows up in the spectra belonging to a thin disk + corona for a given mass accretion rate.

7. Validity of assumptions

7.1. Heat conduction

In our modelling classical heat conduction is assumed. It is only valid if the conductive flux remains sufficiently small against the maximum transport by free streaming electrons. The relevant ratio is estimated here as 0.16 at the radius of maximal mass flow, constant for smaller radii, and decreasing as $1/r^{-1/2}$ for large radii. All estimates are independent of the central mass. Smaller α -values increase the validity of the approximations.

7.2. Equilibrium between electrons and ions

Our model assumes a one-temperature plasma. Temperature equilibrium between electrons and ions requires that the relevant collision timescale between both species remain small compared to the heating timescale. Their ratio is estimated as 0.27 where the coronal mass flow rate reaches its maximum value, and scales as $r^{-1/2}$. Thus at smaller radii this approximation brakes down and electrons and ions will develop different temperatures.

8. Synchrotron radiation, Compton effect

We have performed estimates on the size of these neglected effects. Synchrotron losses are proportional to the number density of electrons, their kinetic energy, and the square of the magnetic field strength. It is often assumed that the magnetic field is dynamo produced and that its energy density is a fraction $\frac{1}{\beta}$ of the gas pressure. The ratio of synchrotron losses to thermal plasma radiation then becomes a pure function of temperature rising with $T^{3/2}$. The main cooling in our solutions occurs in lower layers at about 1/2 of the final coronal temperature. Under such circumstances, synchrotron radiation remains less than bremsstrahlung for $\beta \geq 4$. Values for β in the literature include $\beta \geq 5$ from energy considerations for ADAFs (Quataert & Narayan 1999b) and $\beta \leq 10$ from direct numerical MHD calculations (Matsumoto 1999, Hawley 2000).

Compton cooling by photons from the underlying disk depends on the mass flow rate in the disk. For a rate equal to the maximal coronal mass flow rate, this Compton cooling approaches about 1/3 of the frictional heating. Compton cooling (and heating) of the corona by radiation from the accretion center depends on the state. In the hard state, taking the example of Cyg X-1 (Gilfanov

et al. 2000), the spectrum yields a Compton equilibrium temperature of $10^{8.5}$ K. From the flux one estimates a Compton energy exchange rate comparable with the frictional heating rate in the corona. This indicates that the true coronal temperature at the peak of the coronal mass flow rate of Fig. 3 could be somewhat smaller. A similar result is obtained for Compton cooling by the central flux during the soft state. The keV-photons efficiently cool the corona heated by friction when the temperature obtained with the pure bremsstrahlung assumption is larger than an estimated $10^{8.5}$ K.

All these cooling mechanisms tend to reduce the peak temperature and mass flow rate in Fig. 3 and shift the minimal transition radius somewhat outwards. Our estimates are only rough and a more quantitative evaluation of these effects has to be done later.

9. Comparison with observations

Our model predicts a relation between the evaporation rate and the inner disk location (function \dot{M} in Fig. 3 and 6). This fact can be compared with observations in two ways: [1] for low mass flow rates in the thin disk a hole should form; the location of the change from accretion via the thin disk to a coronal flow should be related to the mass flow rate as predicted; [2] the spectral changes hard/soft and soft/hard should occur for a predicted mass flow rate and the location of the inner edge at this time should agree with that from the model. To perform test [1] we need to know two quantities, the mass flow rate in the thin disk and the inner disk edge location. Fitting of the spectrum based on the ADAF model (for a review see Narayan et al. 1998) gives values of the mass accretion rate on to the black hole and therefore also the evaporation rate (= mass flow rate in the disk at the inner edge). For the location of the inner edge constraints come from the H_α emission line. The maximum velocity indicates the distance of the inner disk edge from the black hole. For test [2] the luminosity for which the spectral transition happens has to be considered, as well as signatures of the inner disk edge.

9.1. Application to X-ray novae

For the X-ray transients A0620-00 and V404 Cyg Narayan et al. (1996,1997a) derived mass accretion rates based on spectral fitting of the ADAF model. These rates were used to perform test [1]. For A0620-00 the resulting inner edge location agrees reasonably with the value from the H_α emission line. For V404 Cyg a discrepancy was found (Meyer 1999), but this disappears with the recent results for V404 Cyg (Quataert & Narayan 1999b) and we find agreement also for this system. The comparison for GRO J1655-40 using the rate from Hameury et al. (1997) and outer-disk-stability arguments is satisfactory. For details of these comparisons see Liu et al. (1999).

The agreement of results derived from the disk evaporation on one side and the ADAF spectral fitting, including different physics for the description of the innermost region, on the other side, supports both models.

Further agreement (related to test [1]) between observation and theoretical modelling of evaporation comes from the computed disk evolution of A0620-00 (Meyer-Hofmeister & Meyer 1999). The long lasting outburst makes plausible that only little matter is left over in the disk. If this is the case the evolution during quiescence can be considered independent of the detailed outburst behaviour. We took into account the evolution of the thin disk together with the corona. The evaporation determines the inner edge of the thin disk at each time. The mass flow rate there is important for the disk evolution and therefore for the outburst cycle (without careful treatment of the inner edge boundary the evolution cannot be determined adequately). The evolution based on the same frictional parameter as taken for dwarf nova modelling ($\alpha_{\text{cool}}=0.05$), leads to the onset of an outburst after the right time and the amount of matter stored in the disk in agreement with the energy estimated from the lightcurve.

Concerning test [2] spectral transitions observed for a few transients can be considered. The best observed source is Nova Muscae 1991 (Cui et al. 1997). The transition occurs around $L_X \approx 10^{37}$ erg/s (Ebisawa et al. 1994). These spectral transitions were modelled based on an ADAF by Esin et al. (1997). Our value for the critical mass accretion rate for a $6 M_\odot$ black hole, $10^{17.2}$ g/s, corresponds to a standard accretion disk luminosity of about $10^{37.2}$ erg/s, in agreement with observations.

9.2. Application to high-mass X-ray binaries

The accretion rates observed for high-mass X-ray binaries are higher than those for transients, fluctuations are common. Therefore hard/soft and soft/hard spectral transitions occur much more often than for transients where this phenomenon is only related to outburst onset or decline. In our investigation of spectral transitions (Meyer et al. 2000) we discuss the behaviour of the three persistent (high-mass) black hole X-ray sources LMC X-1, LMC X-3 and Cyg X-1. The transition occurs around $L_X \approx 10^{37}$ erg/s as also for transients (Tanaka 1999). For the spectral transitions of Cyg X-1 again the ADAF model was successfully used to describe the observations (Esin et al. 1998).

Our model predicts the inner edge of the thin disk at some 100 Schwarzschild radii for the accretion rate related to the hump in Fig. 6, that is at the moment of spectral transition. We have estimated the timescale on which a standard accretion disk at accretion rates near the critical value \dot{M}_{crit} and at the related radius can evaporate or form newly and find a value of the order of days. This agrees with the timescale for the observed spectral transition of a few days for Cyg X-1 (Zhang et al. 1997). Fre-

quency resolved spectroscopy of Cyg X-1 (Revnivtsev et al. 1999) also leads to an inner edge of the thin disk at 150 Schwarzschild radii. But the existence of a reflecting component indicates a disk further inward (Gilfanov et al. 1998, Zycki et al. 1999). For a sample of X-ray transients and high-mass X-ray binaries Di Matteo & Psaltis (1999) found, if they relate the rapid variability properties to those of neutron stars, that the disk reaches down to about 10 Schwarzschild radii. This would be in contrast to the prediction from the ADAF based modelling and our evaporation model. Further work is needed to understand these signatures of a thin disk so far inward during the hard state.

9.3. Application to AGN

Liu et al. (1999) used the results derived in the present paper to predict the location of the inner edge of the thin disk around M87 (test [1]). Using the accretion rate derived by (Reynolds et al. 1996) and an inner edge of the thin disk from emission lines broadening (Harms et al. 1994) they found good agreement between theory and observations.

In connection with new observations further applications of the evaporation model can be discussed (Liu, Meyer and Meyer-Hofmeister, in preparation). Recently the concept of advection-dominated accretion was also applied to the low-luminosity active galactic nuclei M81 and NGC 4579 (Quataert et al. 1999), NGC 4258 (Gammie et al. 1999) and low-luminosity elliptical galaxies (Di Matteo et al. 1999, 2000). It is not clear why for accretion rates which are different by about less than a factor of ten (scaled to Eddington accretion) the thin disks are truncated at $\geq 10^4$ Schwarzschild radii or reach inward to $\approx 100 r_s$. Quataert et al. (1999) argued that the difference might be caused by a different way of mass supply for the ADAF.

9.4. Spectra from the standard thin disk plus corona

One might ask whether spectra computed according to our modelling could be used to test our predictions. Such spectra would include radiation from an inner ADAF region and an outer standard thin disk with the transition at a radius according to our $\dot{M} - r$ relation. The spectra determined according to the ADAF model (see e.g. Narayan et al. 1998) use the observational constraints for the inner edge of the cool disk and fit the observed spectra. If the derived rate \dot{M} and the inner disk location agree with our $\dot{M} - r$ relation these already computed spectra are the spectra that our model will yield.

10. Discussion of further aspects

10.1. Magnetic fields

The magnetic nature of friction in accretion disks is now generally accepted, supported by numerical experiments

that show the generation and sustainment of magnetic fields in accretion disks of sufficient electrical conductivity (for a recent study see Hawley 2000). This raises the question whether the neglect of magnetic fields in modelling the corona-disk interaction may not miss important effects.

Such effects are twofold: (a) Where gyro-frequency is large compared to collision frequency electron thermal conductivity is only high along the magnetic field. This can significantly reduce effective thermal conductivity if the magnetic field is tangled. This can be taken into account by reducing the conductivity coefficient κ_0 by the average of $\cos^2\theta$ over horizontal surfaces, where θ is the angle of the magnetic field with respect to the vertical. (b) Magnetic pressure contributes to the pressure support. This can be taken into account by increasing the value \mathfrak{R}/μ by a factor $1 + \frac{1}{\beta}$ in our equations, where the β is the plasma parameter (which may also include turbulent pressure).

We have performed an order of magnitude approximation to the individual terms in the global energy balance. As we will show in separate work this allows to model our numerical results and suggests the following dependence on the parameters α , κ_0 and β .

$$\begin{aligned} T_0 &\propto \frac{\alpha^2}{\kappa_0} \left(1 + \frac{1}{\beta}\right)^3, \\ T_f &\propto \frac{r_s}{r} \left(1 + \frac{1}{\beta}\right)^{-1}, \\ \frac{\dot{M}}{\dot{M}_{\text{Edd}}} &\propto \alpha \kappa_0^{1/2} \left(1 + \frac{1}{\beta}\right) \left(\frac{r}{r_s}\right)^{3/2} T^{5/2}, \end{aligned} \quad (56)$$

where T_0 is the saturation temperature reached at small radii and T_f is the subvirial temperature attained at large radii. The maximum mass flow rate occurs where the two temperatures T_f and T_0 become about equal. This yields the further proportionalities

$$\begin{aligned} \left(\frac{\dot{M}}{\dot{M}_{\text{Edd}}}\right)_{\text{max}} &\propto \frac{\alpha^3}{\kappa_0^{1/2}} \left(1 + \frac{1}{\beta}\right)^{5/2}, \\ \left(\frac{r}{r_s}\right)_{\dot{M}=\dot{M}_{\text{max}}} &\propto \frac{\kappa_0}{\alpha^2} \left(1 + \frac{1}{\beta}\right)^{-4}. \end{aligned} \quad (57)$$

This may serve as a guide on how the results depend on the choice of these parameter values. For values of β discussed in the literature see Sect. 8.

10.2. The α -dependence

For our numerical computations we took $\alpha=0.3$. Values discussed in the literature include 0.1 to 0.3 from spectral fits of ADAF models to soft X-ray transients (Narayan et al. 1996), $\alpha=0.25$ obtained from applying detailed calculations to luminous black hole X-ray binaries (Esin et

al. 1997), and $\alpha=0.1$ obtained from global magnetohydrodynamical simulations of accretion tori (Hawley 2000). The above scaling relation shows how our results change if other α -values are chosen.

10.3. Irradiation

X-ray irradiation can cause a corona above the thin disk (e.g. London et al. 1981). This can interfere with the assumptions underlying the present model. We note that optically thick scattering layers in the inner corona can prevent such radiation to reach the disk surface (e.g. see Schandl & Meyer 1994). This can become a complex situation which requires a detailed analysis to clarify under what circumstances this affects the applicability of our model. In general, models like ours should be good for black hole systems with ADAF type internal accretion. Aspects of formation of a disk corona have been investigated by de Kool & Wickramasinghe (1999). These calculations are more detailed with respect to ionization equilibrium than ours, but do not include thermal conduction, side-wise advection and wind loss in the energy balance. It is therefore difficult to compare with our results.

11. Comparison with Honma’s model

Here we have considered the spatial co-existence of disk and corona and its gradual fading into a corona/ADAF only region at its inner boundary. Honma (1996) in an apparently very different approach considered the effect of a turbulent diffusive heat flow outwards from a hot and mainly non-radiative advection-dominated inner region to an outer cool accretion disk. In his simplified modelling both regions are treated as one disk with radially varying thickness, and optical depth. He found a steep transition in the disk thickness and temperature at a radius that depends on the mass flow rate. In this radially thin transition layer most of the systems luminosity is radiated.

Though at first sight very different, the two approaches have a basic physical similarity, though in an inverted geometry: What is vertical in the disk+corona system is radial in Honma’s approach. Heat generated by friction is conducted outward (downward) from a hot inner (upper) region to a cool outer (lower) region where it is radiated away. In both cases this establishes the condition where the cool disk ends and the hot, ADAF type flow takes over. We note that Honma’s diffusive heat conductivity bears resemblance to the thermal electron heat conductivity. The rapid increase of the cooling with density leads to a similarly steep temperature profile in Honma’s model as at the base of the corona in the disk+corona model.

We have calculated the ratio of Honma’s effective turbulent heat conductivity to that of electron thermal heat conductivity and obtain the value 1/6 for pressure and temperature at the peak of the coronal mass flow rate in Table 1.

We think that the evaporation model is a more realistic description of the transition from the cool disk to an corona/ADAF only flow. In Sect. 2.5 we estimated the radial heat inflow and showed that it is a minor contribution. Generally, the turbulent outward diffusion of specific energy reduces the inward advective transport (which is also diffusive) of energy. Thus the inward flow of energy is somewhat less than the inward flow of mass times the specific energy. Our approximate treatment of the inward flows of mass and energy in the derivations of Eqs. (39) and (46) in effect leads to such a distinction, for radial power laws as discussed by a factor of 2.

In spite of the very different geometry and simplification Honma’s model captures the same physical effect. His conclusion that his results shed light on the soft-hard transitions of black hole accretors is thus substantiated by the disk+corona model, though quantitative differences exist. In Sect. 5 we have already remarked on where the “strong ADAF proposal” agrees with and where it deviates from the results of the disk+corona model. This brings the “strong ADAF proposal”, Honma’s diffusive heat transport model, and the disk+corona model under a common physical aspect and makes a surprising similarity of some of their results understandable.

12. Conclusions

Our model describes the interaction between the geometrically thin accretion disk and the corona above. We have derived simplified equations, which include the relevant processes determining the accretion via the cool disk together with the hot coronal flow which yields the matter supply for the ADAF towards the black hole. We determine the structure of the corona which is in equilibrium with the cool disk. The equilibrium demands the evaporation of a certain amount of matter from the cool disk and we compute the evaporation rate as a function of the distance r from the central black hole. This gives the rate of accretion of matter towards the inner region (part of the matter is lost by a wind). The evaporation efficiency becomes higher with decreasing r , but reaches a maximum at some hundred Schwarzschild radii. For low accretion rates in the cool disk the evaporation uses up all matter at the distance where the evaporation rate is equal to the mass flow rate in the cool disk. The standard thin disk emits a near black body spectrum and, for high enough accretion rates the disk extends inward to the last stable orbit, the total radiation is soft. But if, for lower accretion rates the thin disk is truncated, the coronal flow/ADAF in the inner region provides a hard spectrum.

These features of disk evaporation apply to galactic black hole X-ray binaries (X-ray transients, high-mass X-ray binaries) and also to AGN (truncated disks were found in low-luminosity AGN and elliptical galaxies). The mass accretion rates derived by spectral fits based on the ADAF model and the location of the inner disk (deduced from

observations or determined by the fitting) allow to check the predictions of the model for the location of transition to the coronal flow. These tests show good agreement for most cases of X-ray transients and the features connected with the maximum evaporation efficiency (see Sect. 9). We want to point out that our model gives qualitative results for relations between mass accretion rate, location of disk truncation and spectral transitions rather than exact values. The division in an outer advection-dominated regime and an inner radiation-dominated regime of the coronal structure gives insight to basic features. Computed values for the edge location might differ by a factor of two to three from the "true" values. An investigation of the detailed effect of simplifications in the equations as well as the effect of the α -value and of magnetic fields will be carried out later.

A truncation of the thin disk farther in than 100 Schwarzschild radii is in contrast to the predictions of our model. The reflecting component observed for Cyg X-1 seems to indicate such an inward extent of the thin disk. But, also for Cyg X-1, another investigation of observations leads to an inner edge location near 100 Schwarzschild radii (see Sect. 9). This situation needs further clarification. But also from the theoretical side the possible existence of an "interior" thin disk below a corona in the innermost regions (closer in than the location of the evaporation efficiency maximum, compare Fig. 3) needs further investigation.

For AGN it was found, based on ADAF spectral modelling that the truncation of the thin disk can be at very different distances from the supermassive black hole for mass accretion rates which differ much less (see Sect. 9). Our model only predicts the large distances. Also here additional investigations are needed to understand the physical reason for such divergent results.

Note added after submission of the manuscript: In a parallel investigation, very similar to our approach, Rózańska & Czerny (astro-ph/0004158, A&A in press) have also studied the coronal structure and the transition to an ADAF. They take into account the possibility of different temperatures of electrons and ions and include Compton cooling by the soft radiation from the underlying disk. In our computed models for the parameters $r/r_S^{3/2} > 25 \dot{M}_{\text{Edd}}/\dot{M}$, that means $\log r/r_S \geq 2.25$ (compare Table 1), the energy equilibration time between electrons and ions is shorter than the heating time, thus establishing temperature equilibrium between electrons and ions. For the same parameters also the rate of Compton cooling by the radiation from the underlying disk is small compared to the frictional heating rate and thus negligible.

References

Abramowicz M.A., Czerny B., Lasota J.P. et al., 1988, ApJ 332, 646

- Abramowicz M.A., Chen X., Kato S. et al., 1995, ApJ Letters 438, L37
 Begelman M.C., 1978, MNRAS 243, 610
 Chen X., 1995, MNRAS 275, 641
 Chen X., Abramowicz M.A., Lasota J.P., Narayan R., Yi I., 1995, ApJ 443, L61
 Chen X., Abramowicz M.A., Lasota J.P., 1997, ApJ 476, L61
 Cui W., Zhang S.N., Focke W. et al., 1997, ApJ 484, 383
 de Kool M., Wickramasinghe D., 1999, MNRAS 307, 449
 Di Matteo T., Psaltis D., 1999, ApJ 526, 101
 Di Matteo T., Fabian A.C., Rees M.J. et al., 1999, MNRAS 305, 492
 Di Matteo T., Quataert E., Allen S.W. et al., 2000, MNRAS 311, 507
 Ebisawa K., Ogawa, M., Aoki T. et al., 1994, PASJ 46, 375
 Esin A.A., McClintock J.E., Narayan R., 1997, ApJ 489, 865
 Esin A.A., Narayan R., Cui W. et al., 1998, ApJ 505, 854
 Gammie C.F., Narayan R., Blandford R., 1999, ApJ 516, 177
 Gilfanov M., Churazov E., Sunyaev R., 1998, in: 18th Texas Symposium on Relativistic Astrophysics and Cosmology, eds. A.V. Olinto et al.; World Scientific, p.735
 Gilfanov M.R., Churazov E.M., Revnivtsev M., 2000, MNRAS in press
 Hameury J.-M., Lasota J.-P., McClintock et al., 1997, ApJ 489, 234
 Harms R.J., Ford H.C., Tsvetanov Z.I. et al., 1994, ApJ 435, L35
 Hawley, J., 2000, ApJ 528, 462
 Honma F., 1996, PASJ 48, 77
 Ichimaru S., 1977, ApJ 214, 840
 Katz J., 1977, ApJ 215, 265
 Kley W., Lin D., 1992, ApJ 397, 600
 Liu F.K., Meyer F., Meyer-Hofmeister E., 1995, A&A 300, 823
 Liu B.F., Yuan W., Meyer F. et al., 1999, ApJ 527, L17
 London R., McCray R., Auer L.A., 1981, ApJ 243, 970
 Lynden-Bell D., Pringle J.E., 1974, MNRAS 168, 603
 Matsumoto R., 1999, in: Numerical Astrophysics, eds. S. Miyama, K. Tomisaka, T. Hanawa, Kluwer, Dordrecht, p. 195
 McClintock J.E., Horne K., Remillard R.A., 1995, ApJ 442 358
 Meyer F., 1999, in: Proc. of Disk Instabilities in Close Binary Systems, eds. S. Mineshige and J.C. Wheeler, Universal Academic Press, Kyoto, p.209
 Meyer F., Meyer-Hofmeister E., 1994, A&A 288, 175
 Meyer F., Liu B.F., Meyer-Hofmeister E., 2000, A&A 354, L67
 Meyer-Hofmeister E., Meyer F., 1999, A&A 348, 154
 Mineshige S., Liu B.F., Meyer F. et al., 1998, PASJ 50, L5
 Nakamura K.E., Matsumoto R., Kusunose M., Kato S., 1996, PASJ 48, 76
 Nakamura K.E., Kusunose M., Matsumoto R., Kato S., 1997, PASJ 49, 503
 Narayan R., Yi I., 1994, ApJ 428, L13
 Narayan R., Yi I., 1995a, ApJ 444, 231
 Narayan R., Yi I., 1995b, ApJ 452, 710
 Narayan R., McClintock J.E., Yi I., 1996, ApJ 457, 82
 Narayan R., Barret D., McClintock J.E., 1997a, 482, 448
 Narayan R., Kato S., Honma F., 1997b, ApJ 476, 49
 Narayan R., Mahadevan R., Quataert E., 1998, in: The Theory of Black Hole Accretion Discs, eds. M.A. Abramowicz et al., Cambridge University Press, p.148
 Novikov I.D., Thorne K.S., 1973 in: Black Holes, eds. C. DeWitt and B. DeWitt, Gordon & Breach, p.343

- Piran T., 1978, ApJ 221, 652
Pringle J., 1981, Ann. Rev. Astron. Astrophys. 137
Quataert E., Narayan R., 1999a, ApJ 516, 399
Quataert E., Narayan R., 1999b, ApJ 520, 298
Quataert E., Di Matteo T., Narayan R., 1999, ApJ 525, L89
Raymond J.C., Cox D.P., Smith B.W., 1976, ApJ 204, 290
Rees M.J., Begelman M.C., Blandford R.D. et al., 1982, Nat 295, 17
Revnivtsev M., Gilfanov M., Churazov E., 1999, A&A 347, L26
Reynolds C.S., Di Matteo T., Fabian A.C. et al., 1996, MNRAS 283, L111
Schandl S., Meyer F., 1994, A&A 289, 149
Shakura N.I., Sunyaev R.A., 1973, A&A 24, 337, 1995, ApJ 446, 741
Shapiro S.L., Lightman A.P., Eardly D.M., 1976, ApJ 204, 187
Shmeleva D.P., Syrovatskii S.I., 1973, Solar Physics 33, 341
Sommerfeld A., 1949, Mechanik der deformierbaren Medien, Akademische Verlagsgesellschaft Geest & Portig, Leipzig
Spitzer L., 1962, Physics of Fully Ionized Gases, 2nd edition, Interscience Publ., New York, London
Tanaka Y., 1999, in: Proc. of Disk Instabilities in Close Binary Systems, eds. S. Mineshige and J.C. Wheeler, Universal Academic Press, Kyoto, p.21
Tanaka Y., Shibazaki N., 1996, ARA&A, 34, 607
Zhang S.N., Cui W., Harmon B.A. et al., 1997, ApJ 477, L95
Zycki T., Done C., Smith D.A., 1999, MNRAS 305, 231